On-chip Hyperspectral Detectors for Fluorescence Lifetime Imaging

Ahasan Ahamed^{1*}, Amita Rawat¹, Lisa N McPhillips¹, Laura Marcu², M Saif Islam¹
¹Electrical and Computer Engineering Department, University of California – Davis, California, USA, 95616

²Biomedical Engineering Department, University of California – Davis, California, USA, 95616

ABSTRACT

Fluorescence Lifetime Imaging (FLIM) is a powerful technique that measures the decay time of fluorophores present in tissue samples alluding to their constituent molecules. FLIM has gained popularity in biomedical imaging for applications such as detecting cancerous tumors, surgical guidance, etc. However, conventional FLIM systems are limited by a reduced number of spectral bands and long acquisition time. Moreover, the large footprint, complexity, and cost of the instrumentation make it difficult for clinical applications. In this paper, we demonstrate a reconstruction-based hyperspectral detector that can resolve decay time and intensities in broad spectral ranges while providing high sensitivity, high gain, and fast response time. The hyperspectral detector is comprised of an array of efficient, ultrafast avalanche photodetectors integrated with nanophotonic structures. We utilize different nanostructures in the detectors to modulate light-matter interactions in spectral channels. This allows us to computationally reconstruct the spectral profile of the incoming fluorescence spectrum without the need for additional filters or dispersive optics. Also, the nanophotonic structures enhance efficiency (by a factor of 2 to 10 over different wavelengths) while providing fast response time. An innovative detector design has been employed to reduce the breakdown of the avalanche photodetectors to -7.8V while maintaining high gain (~50) across the spectral range. Therefore, enabling low light detection with a high signal-to-noise ratio for FLIM applications. Added spectral channels would provide valuable information about tissue materials, morphology, and disease diagnosis. Such innovative hyperspectral sensors can now be integrated on-chip capable of miniaturizing the FLIM system and making it a commercially viable tool for clinical use. This technology has the potential to revolutionize the current FLIM system with improved detection capabilities opening doors for new horizons.

Keywords: Hyperspectral Imaging, Reconstruction-based spectroscopy, Photon-trapping nanostructures, Fluorescence lifetime imaging microscopy, Avalanche Photodiodes, On-chip hyperspectral detectors

1. INTRODUCTION

Fluorescence is a property of certain molecules that can absorb a particular energy of photons and subsequently release photons at a lower energy for a brief amount of time. Scientists utilize this property to classify cellular tissue by both their peak emission wavelengths and the lifetime of the emission. This method of imaging is termed Fluorescence Lifetime Imaging Microscopy (FLIM). FLIM has been a crucial tool for researchers in understanding cell biology on a molecular level, as well as driving toward clinical applications. The advantage of FLIM is that it can provide quantitative information about the molecular environment and metabolic state of tissues. The addition of lifetime measurements allows it to discriminate between multiple fluorophores or tissue components. The ability to complement other imaging modalities such as confocal microscopy, OCT, etc., makes FLIM a lucrative technology¹⁻⁴.

Although FLIM has been utilized in many promising applications such as cancer margin detection, pH level indicator, cell morphology, etc., the implementation of FLIM is limited due to the use of sophisticated sensors, expensive equipment, and long processing time^{5–8}. As fluorescence is a fast process (of the order of a few ns), fast sensors are required to record the fluorescence signal. Furthermore, sensitive detectors are necessary to capture the weak fluorescence signal emitting from

*aahamed@ucdavis.edu; phone 1 530 574-2762

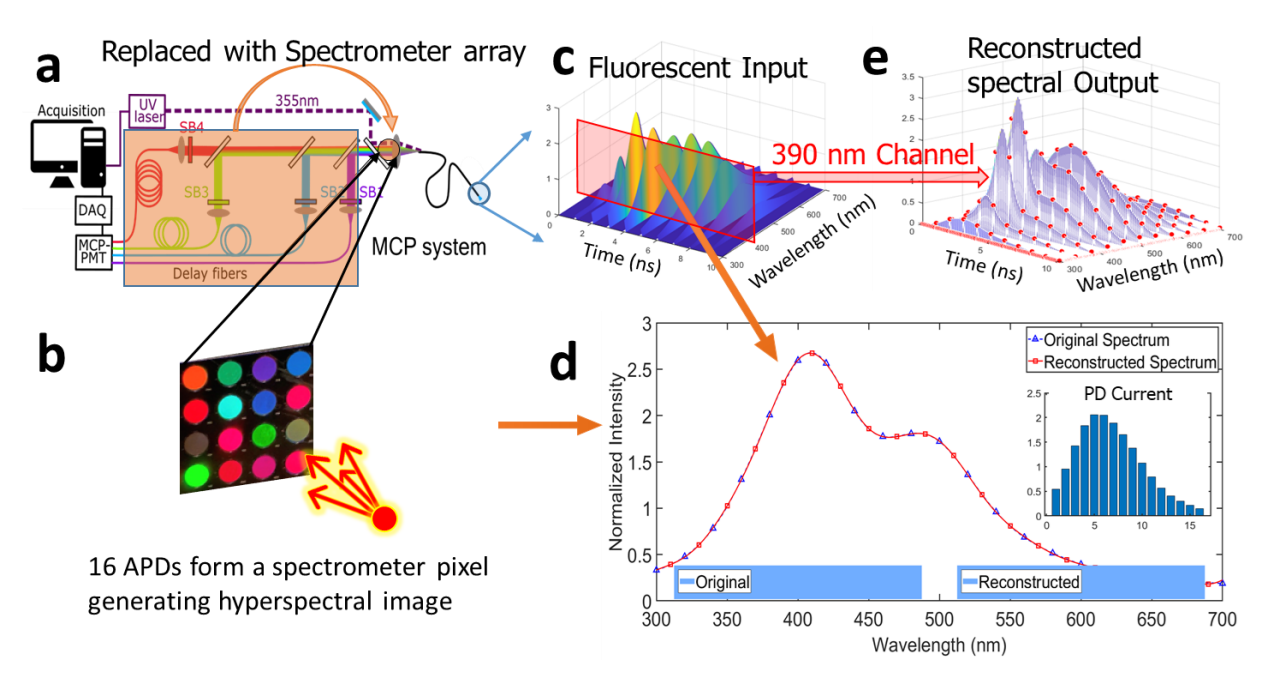


Figure 1: (a) The Schematic of Multi-Chanel Plate (MCP) system setup used in a conventional Fluorescence Lifetime Imaging Microscopy (FLIM) measurement³³. Fluorescent input is generated using a 355 nm ultraviolet (UV) excitation pulse and then collected through the same fiber. The fluorescent spectrum is then split into 4 different channels (390/40 nm, 470/28 nm, 542/28 nm, and 629/53 nm) using delay fibers and is fed into a Photomultiplier Tube (PMT) array for detection. (b) Schematic of 1 pixel spectrometer array setup where 16 avalanche photodiodes. In the proposed setup in will replace the PMT and the delay fibers to detect and stratify different wavelength channels at the same time. (c) Time sampled fluorescence input spectrum released by the tissue after the excitation pulse. (d) The original (blue triangle) and reconstructed (red circle) spectra for the fluorescent input at time = 4 ns. The inset on the right shows the current at different photodiodes (PD). The inset at the bottom shows the color of the original and reconstructed spectrum. (e) The reconstructed spectral output sampled at different channels. This shows how the micro-spectrometer array can be utilized to increase the number of fluorescence channels detected and perform hyperspectral profiling of the fluorescent spectrum.

the tissue. Several efforts have been made to address these challenges. Urayama et al. developed instrumentation for FLIM with picosecond resolution using intensified CCDs⁹. Ulku et al. built a gated 512×512 single-photon SPAD imager for phasor-based widefield FLIM achieving a readout rate of up to 98 kfps¹⁰. Ma et al. developed high-speed compressed sensing to record a widefield lifetime image, eliminating motion artifacts¹¹.

With the advancement of sensors and imaging technology, new research areas are explored. One of the major research interests for FLIM is capturing endogenous fluorophores, and depending on the tissue composition, the fluorescence can have multiple peak emission wavelengths. Therefore, multispectral FLIM has been investigated by several researchers. Although there is adequate sensor technology available to observe fluorescence in a particular wavelength emission, sensor technology lacks in monitoring multi or hyper-spectral FLIM in real-time. De Beule et al. and others developed a hyperspectral FLIM probe setup using dispersive optics^{12–16}. Multi-channel plate photo-multiplier tubes (MCP-PMT), Avalanche Photodiodes (APDs), Single Photon Avalanche Diodes (SPADs), etc. are explored with filters or delay fibers that can observe up to only four spectral channels simultaneously in real-time^{17–20}. However, a convenient miniaturized solution is needed for emerging handheld applications such as real-time surgical guidance, in-vivo drug uptake monitoring, etc.

In this paper, we propose an on-chip detector technology that can provide hyperspectral FLIM with high accuracy and speed. APDs are commonly used in FLIM instrumentations due to their high signal-to-noise ratio and high quantum efficiency 18,19,21,22. Photon-trapping nanostructures have been demonstrated to improve the quantum efficiency, speed, and

gain of the detectors^{23–25}. These photon-trapping nanoholes can modulate the light-matter interaction in the photodiode resulting in enhanced and unique responsivity of the detectors. This property is exploited with the advancement of computational power, to perform reconstruction-based spectroscopy utilizing multiple APDs^{26,27}. This on-chip sensor can be utilized as a replacement for detectors in conventional multi-spectral FLIM setups as shown in Figure 1 making it a compact, cheaper, and mobile solution. This method allows us to observe more than 100 spectral channels simultaneously giving us better insight into the tissue components and endogenous fluorophores. Complementing this technology with conventional FLIM techniques, such as pulse sampling, time-correlated single photon counting, etc., a complete FLIM instrumentation with hyperspectral imaging capabilities is possible. Furthermore, the utilization of photon-trapping nanostructures enhances external quantum efficiency by 2-10 folds²⁸ and improves the detector sensitivity to low light by providing high gain (~50) at only 7.8V reverse bias voltage. Also, these devices have been demonstrated to perform up to 20 GHz bandwidth with less than 30 ps full width at half maximum (FWHM)²⁴. Such detector technology can open up new advent of research in FLIM by providing multi-dimensional information about tissue components and their environments.

2. METHODS AND PROCEDURE

2.1 Fabrication of APDs with photon-trapping structures

The APDs are fabricated on a silicon-on-insulator (SOI) wafer substrate. The doping layers were designed and epitaxially grown by a commercial vendor. Then photon-trapping nanostructures were etched on silicon by Deep Reactive Ion Etching (DRIE) and passivation. Afterward, the top and bottom mesa were etched, and contacts were formed. Silicon-di-oxide was deposited using Plasma Enhanced Chemical Vapor Deposition (PECVD) to passivate the sidewalls, and then metal contact pads were deposited using a combination of sputtering and electron beam evaporator. Details on the fabrication are discussed in reference²⁹.

2.2 External Quantum Efficiency and Gain Measurement

We first obtained the external quantum efficiency of the APDs from 640 nm to 1100 nm wavelength range. We used a supercontinuum laser with an acousto-optic filter to modulate a single wavelength peak with \sim 2 nm FWHM to illuminate the detector. The setup was calibrated to provide a fixed power of 10 μ W over all wavelengths.

We note the photocurrents for each detector and calculate the EQE using the formula (1).

$$EQE = \frac{hc}{\lambda} \times \frac{Photocurrent}{optical\ power}$$
 (1)

Here, h is Planck's constant, c is the speed of light in vacuum, and λ is the wavelength of light in vacuum.

Thereafter, the APDs were biased near breakdown, and the multiplication gain at bias voltage, V was measured using the formula (2).

$$Gain(V) = \frac{Photocurrent(V) - Dark\ Current(V)}{Photocurrent(V_{unity}) - Dark\ current(V_{unity})}$$
(2)

Here, V_{unity} is the voltage at which there is no impact ionization, thereby gain is unity. We consider reverse bias voltage, V = -1V to be unity gain voltage as there is no significant change in the dark or photo current in its vicinity³⁰.

Due to the limitations of the filter range, we could not characterize the detectors in the visible wavelength range (400 nm to 650 nm) which is more suitable for FLIM applications.

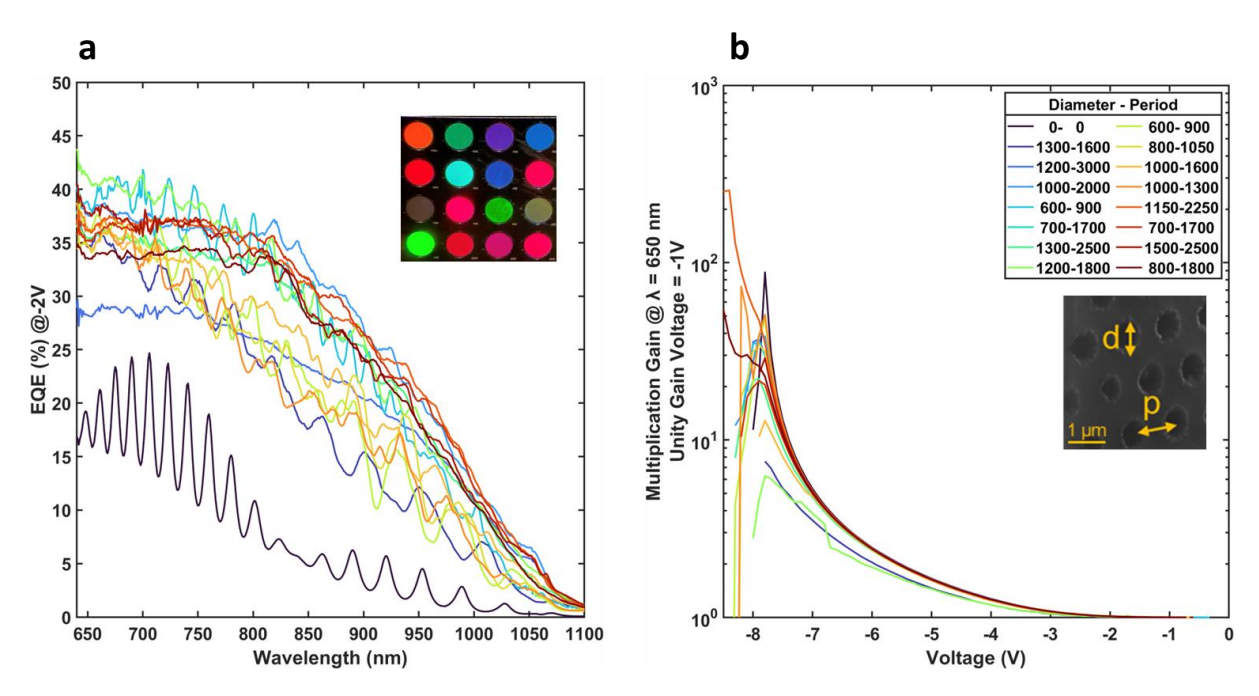


Figure 2: (a) Comparison of the External Quantum Efficiency (EQE) of several avalanche photodiodes with photon-trapping nanoholes. The different diameter and periodicity of the nanoholes modulate the light-matter interaction enabling distinct optical responsivity in the detectors and 2-10 fold increased absorption compared to a flat photodiode (black solid line). (inset) Micrograph of the detectors with photon-trapping nanoholes under ambient illumination, the reflected colors from the detectors further bolster the distinct optical properties due to the effect of nanostructures. (b) The multiplication gains of the avalanche photodiodes over reverse bias voltage measured at 650 nm laser illumination. All of them show high gain of around 50 near breakdown voltage (7.8V). Unity gain is considered as the voltage at which there is no impact ionization. (inset) A Scanning Electron Microscopy (SEM) image of a detector with nanoholes. The diameter, d and periodicity, p is indicated in the image.

2.3 Reconstruction-based spectroscopy

We use a set of 16 EQE data obtained from the measurements as a baseline for detector responsivity. Then, we use synthetically generated spectra and calculated photocurrent using the EQE data to train our computational model to learn the behavior of the detectors. For the training sample, the peak wavelength of the spectra varied from 640 nm to 1100 nm with FWHM varying from 40 nm to 100 nm. After the training, a linear approximation algorithm is used to determine the unknown spectrum from its respective set of photocurrents. Details of the reconstruction algorithm are explained in reference²⁶.

3. RESULTS AND DISCUSSION

3.1 External Quantum Efficiencies and Multiplication Gain

The EQE of the APDs over the wavelength is shown in Figure 3(a). We observe >40% EQE at 640 nm wavelength, and >30% EQE up to 850 nm wavelength in only 1 µm thick absorbing layer APD. Compared with the detector without nanoholes depicted as black solid lines in Figure 2(a), we achieved an EQE enhancement of 2-6-fold in these wavelengths. At longer wavelengths beyond 950 nm, the enhancement is greater than 10 folds. The oscillation in the responsivity curves for detectors with holes is due to the distinctive light-guided mode formation in the silicon caused by the nanoholes. The oscillation is more prominent in detectors with densely packed holes. The oscillations observed in the APD without

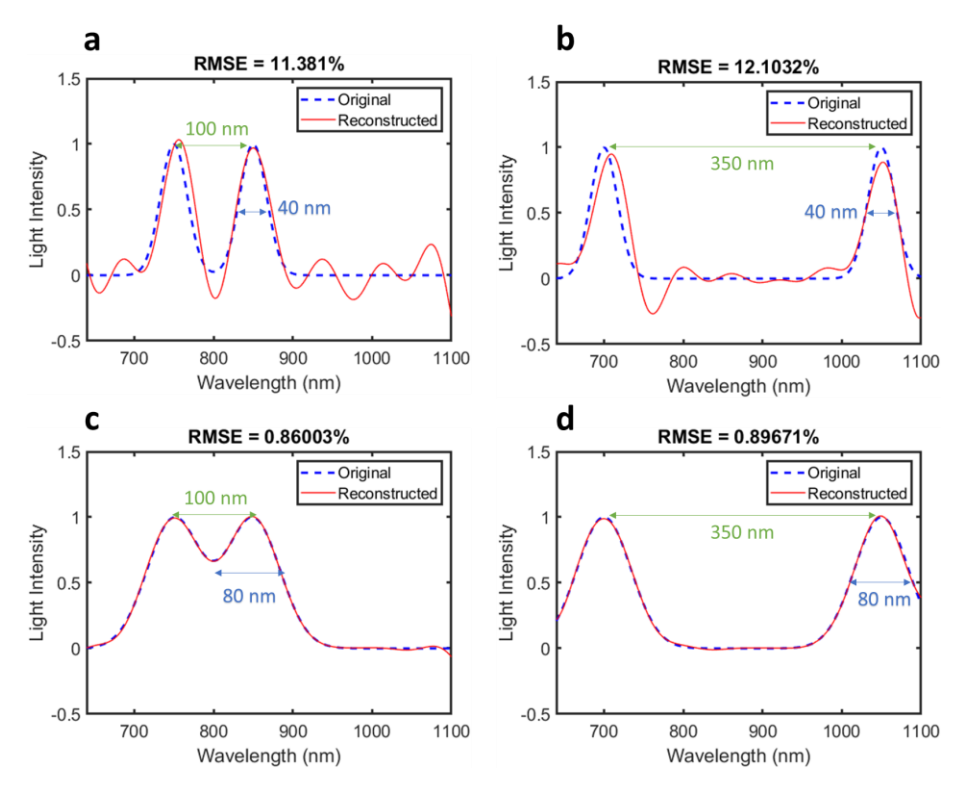


Figure 3: (a-d) Simulated hyperspectral imaging using reconstruction-based spectrometers. The blue dashed line indicates the original spectrum and the red solid line indicate the reconstructed spectrum. Reconstruction is performed for 40 nm full-width at half-maximum (FWHM) in (a-b) with 100 nm and 350 nm separations respectively. It shows a decent reconstruction that can differentiate between the two peaks present in the spectrum. Reconstruction for 80 nm FWHM in (c-d) shows almost accurate reconstruction with less than 1% root mean squared error (RMSE) in both cases of separations.

nanohole are attributed to the vertical resonance of the light between the SOI substrate and the air. However, this resonance phenomenon is not significant in detectors with holes. This distinct responsivity is crucial for making reconstruction-based spectroscopy successful. The optical micrograph of the detectors further bolsters the unique nature of the responsivity with its colorful reflections.

The multiplication gain of the APDs is plotted in Figure 2(b). We observe that most of the APD shows high gain >50 at ~7.8V reverse bias which is the breakdown voltage of the APDs. As the multiplication gain is governed by the electric field profile of the APD, we observe no significant variation in the gain of a flat APD compared to that of an APD with nanoholes. This posits that the electric field profile is not impacted by the etched nanoholes, provided good passivation is done. We observe similar results in our case. Studies suggest that for longer wavelengths, nanostructures improve the penetration depth of photon absorption, thereby improving multiplication gain in APDs^{30,31}. But for 650 nm wavelength, this effect is negligible as it is expected to be efficiently absorbed near the multiplication region. Furthermore, more investigations are necessary to understand the impact of nanoholes in gain manipulation.

3.2 Reconstructed output for hyper-spectral channels

We synthetically generate test fluorescence spectra with two emission wavelength peaks. These peaks are separated by 100 nm and 350 nm and have 40 nm and 80 nm FWHM. These spectra are then fed into the trained reconstruction algorithm, which computationally generates the reconstructed spectra with 461 spectral data points from the set of photocurrents of the APDs as input. The generated reconstructed spectra (solid red line) are shown in Figure 3, compared with the original test spectra (dashed blue line).

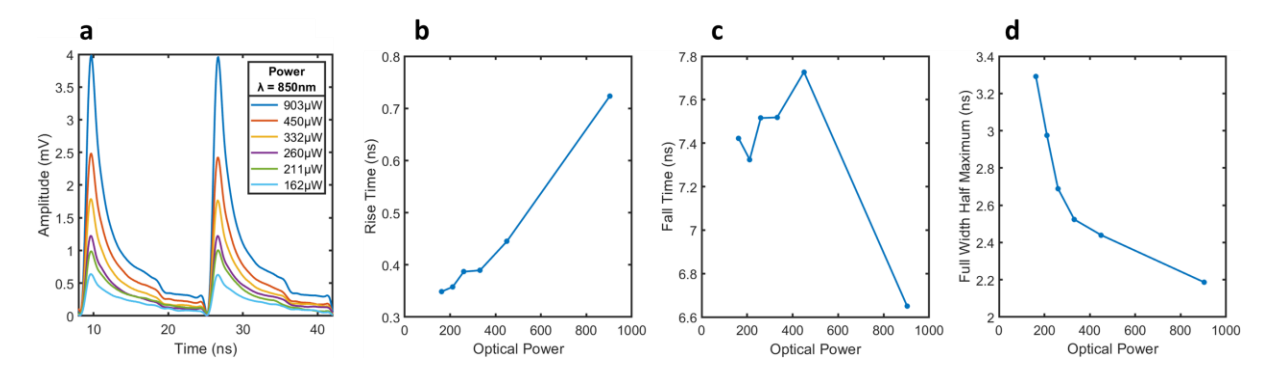


Figure 4: (a) High-speed measurement of an APD with photon-trapping nanoholes with increasing optical power of pulsed laser at 850 nm wavelength. The corresponding (b) rise time, (c) fall time, and (d) full width half maximum (FWHM) is also plotted against the increasing optical power. The rise time increases with increasing power, but the fall time and FWHM drops. We achieve a corresponding 3dB bandwidth of 1 GHz in the detectors that can be used for detecting fluorescence lifetimes.

We observe that in Figure 3(a-b), the reconstruction accuracy is ~90% for FWHM of 40 nm. However, the model could reasonably predict the two wavelength peaks (both amplitude and spectral position). For the broader spectra with FWHM of 80 nm in Figure 3(c-d), the reconstruction accuracy was >99%. The model was able to perfectly predict the wavelength peaks. These results suggest that for broader fluorescent signals, this model will perform perfectly, however, it may find difficulty in reconstructing narrower fluorescent signals (FWHM < 40 nm). This is expected as the model is predicting 461 spectral points from only 16 input data. One way to resolve this is by reducing the number of spectral channels or increasing the number of unique APDs. Another way this can be resolved is by designing a set of detectors with more uniqueness in their responsivity. Also, machine learning algorithms may be employed to achieve better results. Overall, this detector set can provide hyperspectral information of the fluorescent signal in more than 100 spectral channels simultaneously.

To be noted, we performed this reconstruction from 640 nm to 1100 nm wavelength range as the EQE was measured in this range. However, we expect that the EQE at shorter wavelengths such as 400 nm to 650 nm range would have more uniqueness in the EQE spectra and would provide even better hyperspectral reconstruction.

3.3 High-speed measurement

We performed high-speed measurements on the APDs using a pulsed laser source at 850 nm wavelength as an input. The detector response over time is shown in Figure 4. We can see in Figure 4(a) that the detector shows a sharp rise with a long tail. Figure 4(b-d) shows the comparison of rise time, fall time, and FWHM of the impulse response with increasing optical power. Rise time increases with the increasing optical power, this is expected as the number of photons increases, the detector requires more time to capture them effectively. However, the fall time trend does not follow conventional trends, which suggests there may be significant instrument-induced noise in the impulse response. The FWHM decreases with increasing optical power, which further supports the idea of instrument-induced noise. With higher optical power, the impact of noise is reduced. Even then, the detector exhibits a 3dB bandwidth of ~1 GHz calculated using formula (3)³²

$$BW_{3dB} \cong \frac{0.35}{t_{rise}} \tag{3}$$

Where, BW_{3dB} is the 3dB bandwidth of the photodiode, and t_{rise} is the rise time of the impulse response.

Note that, the bandwidth of the detector is limited by the oscilloscope used. We expect higher bandwidth as reported in previous findings²⁴. Therefore, the APD is capable of high-speed acquisition of fluorescence lifetime measurements.

4. CONCLUSION

This on-chip hyperspectral sensor has the potential to revolutionize FLIM instrumentation by miniaturizing the setup circumventing the need for bulky optical parts, narrowband filters, or any additional elements. Furthermore, this can be easily integrated into mobile tools allowing in-situ surgical guidance and real-time monitoring possible. The enhanced efficiency due to photon-trapping structures improves the sensitivity of the detectors, and the gain improves the signal-to-noise ratio enabling better performance of FLIM. Also, reconstruction-based spectroscopy allows these sensors to provide comprehensive spectral information of the fluorescence lifetime, thus providing more accurate information about the tissue compositions and its metabolic activity. This will open up new opportunities in research and clinical applications for FLIM as well as help us get a deep understanding of cellular activity. We believe these sensor arrays will find their application in disease diagnosis, tumor boundary detection, breast cancer surgery, heart pathology, etc.

ACKNOWLEDGEMENTS

This work was supported in part by the UC Davis Engineering Dean's Collaborative Research (DECOR) award, the National Institute of Biomedical Imaging and Bioengineering NCIBT grant # 1-P41-EB032840-01, and the National Science Foundation Award Number 2117424 and PFI-TT 2329884. Part of this study was carried out at the UC Davis Center for Nano and Micro Manufacturing (CNM2).

REFERENCES

- [1] Tinnefeld, P., Buschmann, V., Herten, D.-P., Han, K.-T. and Sauer, M., "Confocal Fluorescence Lifetime Imaging Microscopy (FLIM) at the Single Molecule Level," Single Mol 1, 215–223 (2000).
- [2] Li, C., Bec, J., Zhou, X. and Marcu, L., "Dual-modality fluorescence lifetime imaging-optical coherence tomography intravascular catheter system with freeform catheter optics," J Biomed Opt **27**(07), 076005 (2022).
- [3] Zhou, X., Haudenschild, A. K., Li, C. and Marcu, L., "Multimodal fluorescence lifetime imaging and optical coherence tomography for longitudinal monitoring of tissue-engineered cartilage maturation in a preclinical implantation model," J Biomed Opt **28**(02), 026003 (2023).
- [4] Shrestha, S., Park, J., Pande, P., Applegate, B., Jo Sebina Shrestha, J., Applegate, B. E. and Jo, J. A., "Multimodality optical imaging combining optical coherence tomography (OCT) and fluorescence lifetime imaging (FLIM) for morphological and biochemical tissue characterization," https://doi.org/10.1117/12.841421 **7561**(11), 105–110 (2010).
- [5] Weyers, B. W., Marsden, M., Sun, T., Bec, J., Bewley, A. F., Gandour-Edwards, R. F., Moore, M. G., Farwell, D. G. and Marcu, L., "Fluorescence lifetime imaging for intraoperative cancer delineation in transoral robotic surgery," Transl Biophotonics 1(1–2), e201900017 (2019).
- [6] Bücherl, C. A., Bader, A., Westphal, A. H., Laptenok, S. P. and Borst, J. W., "FRET-FLIM applications in plant systems," Protoplasma **251**(2), 383–394 (2014).

Proc. of SPIE Vol. 12853 1285304-7

- [7] Suhling, K., Hirvonen, L. M., Levitt, J. A., Chung, P. H., Tregido, C., Marois, A. Le, Rusakov, D. A., Zheng, K., Ameer-Beg, S., Poland, S., Coelho, S. and Dimble, R., "Fluorescence lifetime imaging (Flim): Basic concepts and recent applications," Springer Series in Chemical Physics **111**, 119–188 (2015).
- [8] Wang, M., Tang, F., Pan, X., Yao, L., Wang, X., Jing, Y., Ma, J., Wang, G. and Mi, L., "Rapid diagnosis and intraoperative margin assessment of human lung cancer with fluorescence lifetime imaging microscopy," BBA Clin **8**, 7–13 (2017).
- [9] Urayama, P., Zhong, W., Beamish, J. A., Minn, F. K., Sloboda, R. D., Dragnev, K. H., Dmitrovsky, E. and Mycek, M. A., "A UV-visible-NIR fluorescence lifetime imaging microscope for laser-based biological sensing with picosecond resolution," Appl Phys B **76**(5), 483–496 (2003).
- [10] Ulku, A. C., Bruschini, C., Antolovic, I. M., Weiss, S., Michalet, X. and Charbon, E., "Phasor-based widefield FLIM using a gated 512×512 single-photon SPAD imager," Proc SPIE Int Soc Opt Eng **10882**, 21 (2019).
- [11] Ma, Y., Lee, Y., Best-Popescu, C. and Gao, L., "High-speed compressed-sensing fluorescence lifetime imaging microscopy of live cells," Proc Natl Acad Sci U S A **118**(3), e2004176118 (2021).
- [12] De Beule, P. A. A., Dunsby, C., Galletly, N. P., Stamp, G. W., Chu, A. C., Anand, U., Anand, P., Benham, C. D., Naylor, A. and French, P. M. W., "A hyperspectral fluorescence lifetime probe for skin cancer diagnosis," Review of Scientific Instruments **78**(12), 123101 (2007).
- [13] Bednarkiewicz, A., Bouhifd, M. and Whelan, M. P., "Digital micromirror device as a spatial illuminator for fluorescence lifetime and hyperspectral imaging," Applied Optics, Vol. 47, Issue 9, pp. 1193-1199 47(9), 1193–1199 (2008).
- [14] Nie, Z., An, R., Hayward, J. E., Farrell, T. J. and Fang, Q., "Hyperspectral fluorescence lifetime imaging for optical biopsy," J Biomed Opt **18**(9), 096001 (2013).
- [15] Croce, A. C. and Bottiroli, G., "Autofluorescence spectroscopy and imaging: A tool for biomedical research and diagnosis," European Journal of Histochemistry **58**(4), 320–337 (2014).
- [16] Feng Wang, X., Periasamy, A., Herman, B. and Coleman, D. M., "Fluorescence Lifetime Imaging Microscopy (FLIM): Instrumentation and Applications," Crit Rev Anal Chem **23**(5), 369–395 (1992).
- [17] Becker, W., Bergmann, A. and Biskup, C., "Multispectral fluorescence lifetime imaging by TCSPC," Microsc Res Tech **70**(5), 403–409 (2007).
- [18] Zhou, X., Marcu, L., Yankelevich, D. and Bec, J., "Multispectral fluorescence lifetime imaging device with a silicon avalanche photodetector," Optics Express, Vol. 29, Issue 13, pp. 20105-20120 **29**(13), 20105–20120 (2021).
- [19] Lagarto, J. L., Villa, F., Tisa, S., Zappa, F., Shcheslavskiy, V., Pavone, F. S. and Cicchi, R., "Real-time multispectral fluorescence lifetime imaging using Single Photon Avalanche Diode arrays," Sci Rep **10**(1) (2020).

- [20] Sun, Y., Liu, R., Elson, D. S., Hollars, C. W., Jo, J. A., Park, J., Sun, Y. and Marcu, L., "Simultaneous timeand wavelength-resolved fluorescence spectroscopy for near real-time tissue diagnosis," Opt Lett 33(6), 630 (2008).
- [21] Becker, W., Su, B., Holub, O. and weisshart, K., "FLIM and FCS detection in laser-scanning microscopes: Increased efficiency by GaAsP hybrid detectors," Microsc Res Tech **74**(9), 804–811 (2011).
- [22] Bartolo-Perez, C., Chandiparsi, S., Mayet, A. S., Cansizoglu, H., Gao, Y., Qarony, W., AhAmed, A., Wang, S.-Y., Cherry, S. R., Saif Islam, M. and Ariño-Estrada, G., "Avalanche photodetectors with photon trapping structures for biomedical imaging applications," Opt Express **29**(12), 19024 (2021).
- [23] Gao, Y., Cansizoglu, H., Polat, K. G., Ghandiparsi, S., Kaya, A., Mamtaz, H. H., Mayet, A. S., Wang, Y., Zhang, X., Yamada, T., Devine, E. P., Elrefaie, A. F., Wang, S. Y. and Islam, M. S., "Photon-trapping microstructures enable high-speed high-efficiency silicon photodiodes," Nat Photonics (2017).
- [24] Bartolo-Perez, C., Qarony, W., Ghandiparsi, S., Mayet, A. S., Ahamed, A., Cansizoglu, H., Gao, Y., Devine, E. P., Yamada, T., Elrefaie, A. F., Wang, S.-Y. and Islam, M. S., "Maximizing Absorption in Photon-Trapping Ultrafast Silicon Photodetectors," Adv Photonics Res 2(6), 2000190 (2021).
- [25] Ghandiparsi, S., Devine, E. P., Yamada, T., Wang, S. Y., Islam, M. S., Elrefaie, A. F., Mayet, A. S., Landolsi, T., Bartolo-Perez, C., Cansizoglu, H., Gao, Y., Mamtaz, H. H. and Golgir, H. R., "High-Speed High-Efficiency Photon-Trapping Broadband Silicon PIN Photodiodes for Short-Reach Optical Interconnects in Data Centers," Journal of Lightwave Technology (2019).
- [26] Ahamad, A., Ghandiparsi, S., Bartolo-Perez, C., Mayet, A. S., Cansizoglu, H., Devine, E. P., Elrefaie, A. F., Dhar, N. K., Wang, S.-Y., Yang, W. and Islam, M. S., "Smart nanophotonics silicon spectrometer array for hyperspectral imaging," Conference on Lasers and Electro-Optics, STh3M.2, Optical Society of America (2020).
- [27] Ahamed, A., Rawat, A., Mayet, A. S., McPhillips, L. N. and Islam, M. S., "Unique Hyperspectral Response Design in High-Speed Photodetectors Enabled by Periodic Surface Textures," Res Sq (2023).
- [28] Qarony, W., Mayet, A. S., Ponizovskaya-Devine, E., Ghandiparsi, S., Bartolo-Perez, C., Ahamed, A., Rawat, A., Mamtaz, H. H., Yamada, T., Wang, S.-Y. and Islam, M. S., "Achieving higher photoabsorption than group III-V semiconductors in ultrafast thin silicon photodetectors with integrated photon-trapping surface structures," https://doi.org/10.1117/1.APN.2.5.056001 2(5), 056001 (2023).
- [29] Rawat, A., Ahamed, A., Bartolo-Perez, C., Mayet, A. S., McPhillips, L. N. and Islam, M. S., "Design and Fabrication of High-Efficiency, Low-Power, and Low-Leakage Si-Avalanche Photodiodes for Low-Light Sensing," ACS Photonics **10**(5), 1416–1423 (2023).
- [30] Bartolo-Perez, C., Ahamed, A., Mayet, A. S., Rawat, A., McPhillips, L., Ghandiparsi, S., Bec, J., Ariño-Estrada, G., Cherry, S., Wang, S.-Y., Marcu, L. and Islam, M. S., "Engineering the gain and bandwidth in avalanche photodetectors," Opt Express **30**(10) (2022).
- [31] Ahamed, A., Bartolo-Perez, C., Sulaiman Mayet, A., Ghandiparsi, S., Zhou, X., Bec, J., K. Dhar, N., P. Devine, E., Wang, S.-Y., Ariño-Estrada, G., Marcu, L. and Islam, M. S., "Controlling light penetration

- depth to amplify the gain in ultra-fast silicon APDs and SPADs using photon-trapping nanostructures," Proceedings of SPIE The International Society for Optical Engineering **11800** (2021).
- [32] "ELECTRICAL CHARACTERISTICS Photodiode Characteristics Typical Capacitance vs. Reverse Bias.", .
- [33] Yankelevich, D. R., Ma, D., Liu, J., Sun, Y., Bec, J., Elson, D. S. and Marcu, L., "Design and evaluation of a device for fast multispectral time-resolved fluorescence spectroscopy and imaging," Review of Scientific Instruments **85**(3), 34303 (2014).

Proc. of SPIE Vol. 12853 1285304-10